Biomedicine & Pharmacotherapy 191 (2025) 118511

Contents lists available at ScienceDirect

Biomedicine & Pharmacotherapy

journal homepage: www.elsevier.com/locate/biopha

Exploring the multifunctional potential of designed benzothiazole hydrazones

Riccardo Barbari [a,1], Vera Bruggink [c,1], Robert Klaus Hofstetter [c], Chiara Tupini [b], Leonardo Montani [a], Sofia Fagnani [b], Filippo Marchetti [a], Elisa Durini [a], Ilaria Lampronti [b], Silvia Vertuani [a], Anna Baldisserotto [a,*], Oliver Werz [c,*], Stefano Manfredini [a]

[a] Department of Life Science and Biotechnology, Section of Medicines and Health Products, University of Ferrara, via Fossato di Mortara 17-19, Ferrara I-44121, Italy
[b] Department of Life Science and Biotechnology, Section of Biochemistry and Molecular Biology, University of Ferrara, via Fossato di Mortara 74, Ferrara I-44121, Italy
[c] Department of Pharmaceutical/Medicinal Chemistry, Institute of Pharmacy, Friedrich Schiller University Jena, Jena 07743, Germany

ARTICLE INFO

Keywords:
Antioxidant
Multifunctional
Anti-inflammatory
Skin-desease
Eterocycle

ABSTRACT

The involvement of oxidative stress in the aetiology of various multifactorial diseases is well known, just as the design of multifunctional compounds is recognized as an innovative strategy to control complex-spectrum diseases. The purpose of this work was to synthesize a small library of six benzothiazole derivatives with hydrazonic spacers and to evaluate their multifunctional efficacy in terms of antioxidant, UV-filtering, antiproliferative, and anti-inflammatory activities. From the SAR study it emerged that the hydrazone linker, when coupled with a hydroxyl group in position 4 and another hydroxyl or methoxyl in position 3, seems to direct the profile of the molecule towards multifunctionality. The antitumor activity against melanoma cells seems to be related to the inhibition of tyrosinase (**BZTidr10–12**). All the compounds of the series have shown to be direct inhibitors of 5-lipoxygenase (5-LO). In particular, compound **BZTidr12**, with an IC_{50} of 0.03 μM, proved to be the most potent inhibitor of the series against isolated 5-LO activity in a cell-free assay.

1. Introduction

Multifactorial diseases, which involve multiple biological pathways and complex pathophysiological issues, pose significant treatment challenges. Combination therapies targeting individual pathways or symptoms often raise concerns about cost, patient adherence, and adverse drug interactions, potentially diminishing efficacy and increasing side effects [1–3]. Multifunctional compounds combine several multiple biological activities into a single molecule, potentially offering enhanced therapeutic effects by simultaneously targeting various disease pathways while reducing adverse effects [4–6]. The design of multifunctional compounds is of significant interest for the treatment of diseases that lack adequate therapeutic options to date.

Skin cancers—including melanoma and non-melanoma forms—are a widely disseminated and multifactorial group of diseases that represent a promising area of application for multifunctional compounds. Skin cancer incidence is rising due to the depletion of the ozone layer and increased exposure to ultraviolet (UV) radiation [7], with UVA-induced reactive oxygen species (ROS) damaging DNA and potentially causing mispairing, mutations, and uncontrolled cell proliferation [8–10]. UV exposure also activates pro-inflammatory processes that contribute to skin cancer development [11–13]. Our research aims at developing multifunctional compounds for the prevention and treatment of skin diseases such as melanoma by focusing on new chemical entities that combine broad-spectrum photoprotection, antioxidant activity, anti-inflammatory effects, and antiproliferative properties. 2-Phenyl-1-H-benzimidazole-5-sulfonic acid (PBSA)—a well-established UVB filter—was chosen as a lead compound, though it lacks UVA protection and antioxidant properties. Structural modifications implemented in previous studies have generated bioisosteric analogs of PBSA with

* Corresponding authors.
E-mail addresses: brbrcr@unife.it (R. Barbari), vera.bruggink@uni-jena.de (V. Bruggink), robert.klaus.hofstetter@uni-jena.de (R.K. Hofstetter), chiara.tupini@unife.it (C. Tupini), leonardo.montani@unife.it (L. Montani), sofia.fagnani@unife.it (S. Fagnani), filippo.marchetti@unife.it (F. Marchetti), dre@unife.it (E. Durini), lmi@unife.it (I. Lampronti), vrs@unife.it (S. Vertuani), bldnna@unife.it (A. Baldisserotto), oliver.werz@uni-jena.de (O. Werz), smanfred@unife.it (S. Manfredini).
[1] These authors contributed equally to this work

https://doi.org/10.1016/j.biopha.2025.118511
Received 13 May 2025; Received in revised form 4 August 2025; Accepted 25 August 2025
Available online 28 August 2025

enhanced biological activities, where (i) the benzimidazole core is replaced by other heterocycles, (ii) the length and nature of the linker bridge have been explored, and (iii) the phenyl ring has been decorated with different functional groups. By screening libraries of benzofuran hydrazones, indole hydrazones, benzimidazole hydrazones, 2-arylbenzimidazoles, 2-arylbenzothiazoles and benzothiazole derivatives, several promising candidates were identified with improved antioxidant, photoprotective and antiproliferative properties [14–20].

Recently our focus turned towards the benzothiazole scaffold, a structure widely represented in antimicrobial, anticancer, anticonvulsant, neuroprotective, anti-inflammatory, and antioxidant drug candidates [21–29]. Based on previous screening results, our current aim was the synthesis and characterization of a small library of benzothiazole hydrazone derivatives as potential multifunctional agents for the prevention and treatment of skin-related diseases, and the investigation of their SAR profile regarding the influence of different spacers and substituents on bioisosteric cores, thereby combining the results of this series with those of previous investigations.

Sunscreens are traditionally assessed by their capacity to absorb ultraviolet (UV) radiation and prevent erythema; however, emerging research reveals the critical need for formulations that also mitigate UVA-induced oxidative stress and downstream inflammatory responses. UVA radiation penetrates deeper into the dermis compared to UVB, generating ROS that provoke lipid peroxidation, DNA damage, and activation of pro-inflammatory signaling pathways, including the 5-lipoxygenase (5-LO) pathway [30,31]. Conventional single-molecule UV filters such as avobenzone provide effective UVA protection but lack intrinsic antioxidant or anti-inflammatory properties [32]. Meanwhile, natural antioxidants like ferulic acid exhibit marked radical-scavenging activity [33], yet their application is limited due to rapid photodegradation and insufficient UVB absorption. By integrating a benzothiazole chromophore—known for strong absorption in the UVA and UVB spectra [34]—with a redox-active hydrazone linker capable of reducing ROS formation and inhibiting 5-LO-mediated inflammation, our hybrid molecules strategically address both photoprotective and pharmacological gaps. This dual-action design potentially offers improved broad-spectrum photoprotection alongside anti-inflammatory efficacy, fulfilling a significant unmet need in topical photoprotection technologies.

2. Results and discussion

2.1. Chemistry

Spurred by the promising results of previously disclosed benzothiazole acylhydrazones derivatives (**BZTidr1–6**) [20], we synthesized a library of benzothiazol hydrazones (compounds **BZTidr7-12**) by an adequate shortening of the linker system, previously adopted in order to keep a minimal π-conjugated carbon-nitrogen atom sequence on the linker (Scheme 1) in order to complete the SAR profile of these 12 hydrazone derivatives and evaluate the influence of the two different linkers. Target compounds were synthesized as shown in Scheme 2: starting material 2-aminothiophenol (**1**) was treated with potassium thiocyanate in strong acidic aqueous medium, at reflux condition, for

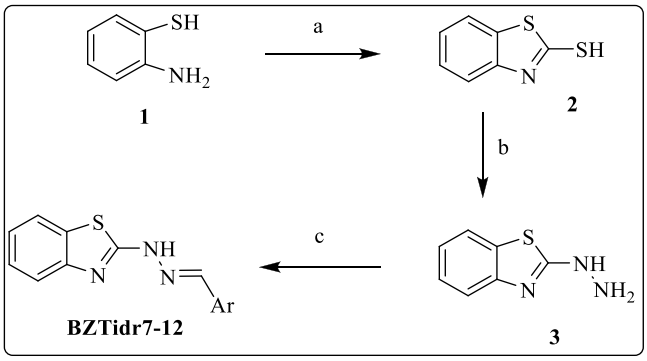

Scheme 2. Synthetic route to compounds **BZTidr7–12**. Reagents and conditions: a) KSCN, HCl 4 N, 24 h, reflux. b) $N_2H_4{\cdot}H_2O$ (25 % w/w), abs. EtOH, 48 h, reflux. c) Ar-CHO, EtOH, 2–5 h, 60°C.

24 h to afford 2-mercaptobenzo[*d*]thiazole (**2**). After recrystallization, it was reacted with a solution of hydrazine hydrate, at reflux condition, for 48 h, delivering the required intermediate 2-hydrazinobenzo[*d*]thiazole **3** in good yield. Finally, target compounds **BZTidr7–12** were obtained in almost quantitative yield from classical amine-aldehyde condensation in EtOH, at 60 °C, for 2–5 h. All the synthesized compounds were in agreement with expected analytical data: identification of target benzothiazole hydrazones was achieved through spectroscopic techniques FT-IR, ^{1}H-NMR and ^{13}C-NMR; the purity was assessed through HPLC-UV analysis (spectral data are given in the Supporting Information). Appearance of a strong C═N stretching band between 1598 and 1625 cm^{-1} was observed in final products, diagnostic for the formation of an azomethine bond. In the ^{1}H-NMR spectra of compounds **BZTidr7–12** chemical shift values for the -NH- and -OH protons fall in the range 11.97–12.06 ppm and 9.20 – 9.86 ppm, respectively. According to the literature, the presence of a singlet downfield resonating signal in the range 8.27–8.87 ppm, relative to the proton of the azomethine group, exclusively accounts for formation of E-isomers [35].

2.2. Antioxidant activity

Comprehensive antioxidant compound profiling requires several assays, since antioxidant effects can be the result of multiple mechanisms [36]. All synthesized compounds were therefore evaluated in three different antioxidant assays, encompassing two different *in vitro* single electron transfer (SET) methods – namely 1,1-diphenyl-2-picrylhydrazyl radical-scavenging activity (DPPH) and ferric reducing antioxidant power (FRAP) – as well as one *in vitro* hydrogen atom transfer (HAT) method (oxygen radical absorbance capacity (ORAC)) [37]. Antioxidant activity data are summarized in Table 1. For FRAP and ORAC assays, data are expressed as micromoles of Trolox equivalents per gram of sample (μmolTE/g), whereas for better interpretation of results from the DPPH assay, values are reported as IC_{50}.

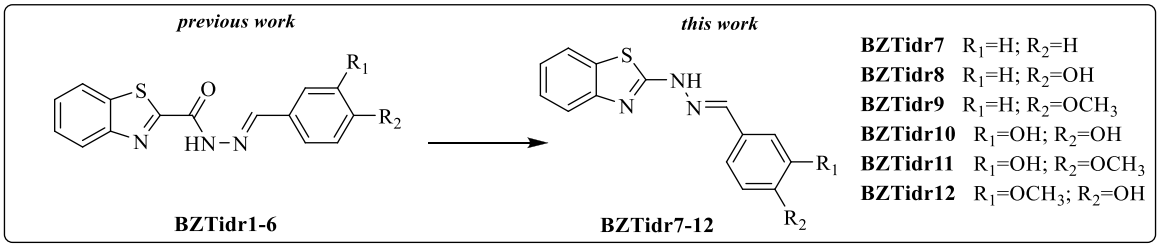

Scheme 1. Design of benzothiazole hydrazones **BZTidr7–12**.

Table 1
Antioxidant activity of benzothiazole hydrazones **BZTidr7-12**.

Compound	Ar	DPPH[a] IC_{50} (μg/mL)	FRAP[a] (μmolTE/g)	ORAC[a] (μmolTE/g)
BZTidr7	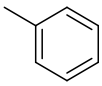	18.48 ± 1.28	2354.91 ± 172.86	<LOQ[b]
BZTidr8	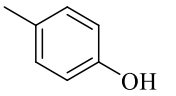	13.57 ± 0.59	7176.12 ± 180.61	27,607.86 ± 129.71
BZTidr9	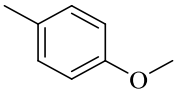	22.32 ± 2.27	2211.22 ± 22.76	2526.80 ± 19.96
BZTidr10	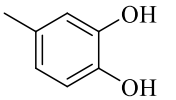	4.66 ± 0.54	11117.52 ± 561.97	9446.17 ± 65.04
BZTidr11	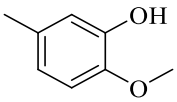	27.40 ± 0.32	2408.06 ± 200.97	9816.83 ± 555.75
BZTidr12	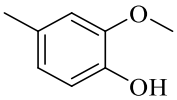	100.86 ± 5.78[c]	4803.96 ± 369.13	23,250.54 ± 1169.01
BZTidr4	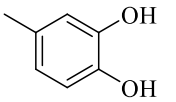	3.27 ± 0.21	5506.15 ± 120.52	not available
Ferulic Acid	-	9.90 ± 0.7	6872.60 ± 10.7	15,906.40 ± 14.2

[a] Each value is the mean of at least three independent experiments (N ≥ 3, mean ± SD).
[b] Below limit of quantification.
[c] Staining formation observed.

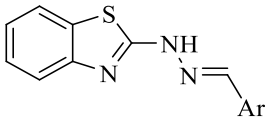

The series displayed excellent radical scavenging activity, with DPPH inhibition around 90 % for all compounds even at 0.1 mg/mL (data not shown). Subsequent IC_{50} analyses revealed values in the low single- or double-digit micromolar range for all compounds, highlighting this class's exceptional antioxidant and radical scavenging potential. An exception is the 3-methoxy-4-hydroxybenzilidene derivative **BZTidr12**, where a persistent yellow/orange stain that hampered absorbance detection. Because most derivatives showed similar activity regardless of substitution pattern, we hypothesize that the linker structure may negatively affect antioxidant capacity. The presence of an electron-withdrawing group (EWG) in para position appears beneficial, likely by enhancing electron delocalization on the aromatic ring. Indeed, the 4-hydroxybenzilidene derivative **BZTidr8** and the 3,4-dihydroxybenzilidene derivative **BZTidr10** exhibited the lowest IC_{50} values of the series, with the latter surpassing even the efficiency of the reference compound ferulic acid ($p = 0.0139$). The profile of **BZTidr10** is similar to that of **BZTidr4** in the acyl-hydrazon series ($p = 0.0770$), confirming that the catecholic function, in both cases, provides considerable antioxidant activity. Conversely, an electron-donating group (EDG) in the same position might hinder delocalization; thus, hydrazones **BZTidr9** and **BZTidr11**, each bearing a -OMe group in para position, display slightly higher IC_{50} values compared to the other series members, such as **BZTidr7**, which has no substituent ($p = 0.1263$ and $p = 0.0107$, respectively). The antioxidant activity observed in the FRAP test was consistent with the DPPH results. Thus, all tested compounds demonstrated remarkable potency, and **BZTidr8**, **BZTidr10**, and **BZTidr12** showed the highest values in the series (with highly statistically significant *p*-values against the other compounds in the series, ranging from $0.0266 < p < 0.0001$), suggesting that an EWG group in para position can facilitate electron delocalization and enhance overall antioxidant efficacy.

The ORAC test was carried out to confirm the antioxidant data and to extend the activity profile of the candidates. Except for hydrazone **BZTidr7**, which showed no activity, all derivatives demonstrated the ability to quench peroxyl radicals, thereby preventing the oxidative degradation of fluorescein. The 4-methoxybenzilidene derivative **BZTidr9** exhibited weak radical quenching properties, while hydrazone derivatives **BZTidr8** and **BZTidr12** proved to be the best performing candidates in this assay, surpassing even the efficiency of the potent antioxidant ferulic acid ($p = 0.0001$ and $p = 0.0004$, respectively). Indeed, compound **BZTidr8** produced an outstanding value of 27,607 ± 130 μmol TE/g, which was one of the highest ever recorded by our group for a synthetic antioxidant molecule. Unexpectedly, the 3,4-dihydroxybenzilidene derivative **BZTidr10**, despite having the best performance in other assays, displayed good antioxidant capacity, which is, however, modest compared to **BZTidr8** and **BZTidr12** ($p = 0.0001$ and $p = 0.0005$, respectively).

The discrepancies between the DPPH/FRAP values and ORAC values are most likely due to the different mechanisms involved. In SET-based reactions, dissociation of the phenolic proton is crucial for subsequent electron transfer, so the presence of an EWG near the hydroxyl moiety facilitates this step. In contrast, in HAT-based mechanisms, the hydrogen atom transfer can be slightly hindered by an EWG but enhanced by an adjacent EDG, such as a methoxy group.

2.3. Evaluation of in vitro UV-filtering parameters

2.3.1. UV-filtering parameters in solution

As the UV absorbance capacity is strictly related to the sunscreen performance of a UV filter and to its sun protection factor (SPF), the maximum absorption wavelength (λ_{max}) and the molar extinction coefficient (ε) of each derivative in DMSO:MeOH solution were evaluated and their absorption spectra recorded (Figure S1). Benzothiazole hydrazone derivatives **BZTidr7–12** (Table 2) showed very similar absorption spectra profiles among each other. Their λ_{max} falls in the UVA range between 333.40 (**BZTidr7**) and 342.30 nm (**BZTidr12**) and their ε is calculated in the range 38,569.62–43,456.09. Those values confirm the high UV absorption capacity of this class of benzothiazole derivatives, which seems to be related to the linker structure, rather than to the number and nature of substituents on the aryl moiety.

A slight bathochromic effect can be noted for compounds **BZTidr9** and **BZTidr11**, bearing a methoxy group in position 4 of the aromatic

Table 2
Spectral data from spectrophotometric analysis of benzothiazole derivatives **BZTidr7-12**.

Compound	λ_{max} (nm)	ε[a] ($dm^3\ mol^{-1}\ cm^{-1}$)
BZTidr7	333.3	38,569.62
BZTidr8	337.5	38,706.20
BZTidr9	336.8	43,456.09
BZTidr10	341.4	39,017.09
BZTidr11	340.3	43,218.56
BZTidr12	342.3	39,206.59
PBSA	*304.5*	*23,881.86*

[a] Calculated by applying the Lambert-Beer equation with the absorbance recorded at λ_{max}.

ring: those derivatives were the only ones that displayed Ɛ values above 40,000, almost doubling the Ɛ of reference UVB filter PBSA that does not show any absorption in the UVA region, as suggested by its λ_{max} of 304.50 nm. It can therefore be deduced that for these derivatives the inclusion of an EDG group in para position can moderately increase the UV absorption capacity of the candidate filter.

2.3.2. UV-filtering parameters in formula

Pursuing the aim of developing multifunctional compounds with multiple biological activities, the synthesized benzothiazole hydrazones were evaluated for potential sunscreen application. All candidates were incorporated in a suitable cosmetic formulation at 3 % and their photoprotective efficacy evaluated using the Diffey-Robson method [38]. The formulation consists of a standard O/W emulsion suitable for sunscreen application: each benzothiazole derivative was heat-solubilized in a standard oil-phase, then dispersed into the formulation at the same temperature using a turbo emulsifier and mixed until cooling. The emulsion was then spread on polymethylmethacrylate plates (PMMA) prior to recording the transmittance spectra. The UV-filtering parameters to evaluate efficacy requirements for potential sunscreen applications, namely SPF value, UVA protection factor value (UVAPF), the UVA/UVB ratio, and the critical wavelength (λc), were obtained from elaboration of the transmittance spectra using SPF calculator software and are listed in Table 3.

According to the Food and Drug Administration [39], a sunscreen, to be considered broad-spectrum, and thus able to protect the skin from both UVA and UVB rays, should have a λc value above 370 nm: all the compounds listed in Table 3 could therefore be classified as broad-spectrum. According to EU guidelines [40] a sunscreen product must have minimum efficacy requirements including an SPF value of 6 (or higher), a UVA/UVB ratio of 1/3, and a critical λ value (λc) greater than 370 nm. Although none of the compounds met the minimum SPF criterion at the concentration tested, they all fully met the other two requirements and showed noteworthy values compared to the commercial filter PBSA. It should be noted, in particular, that all compounds exhibit a UVA/UVB ratio greater than 1, far above the threshold value established by the EU. These values reflect the tendency of benzothiazole derivatives to absorb UV light preferentially in the UVA range, making them suitable for broad-spectrum photoprotection applications. The presence of auxochromic groups at the para position, such as hydroxyl, enhances the filtering ability of benzothiazole hydrazone derivatives, as evidenced by the higher SPF and UVAPF values recorded for compounds **BZTidr8**, **BZTidr10** and **BZTidr12**, underlining a greater contribution of the hydrazonic linker to this activity than the former acyl-hydrazonic (**BZTidr4**).

2.3.3. Photostability

A sunscreen must be accompanied by photostability data that can be obtained, according to criteria established by Garoli et al. [41], by recording pre- and post-irradiation transmittance spectra (in the range of 290–400 nm) of PMMA plates with finger-coat formulations subjected to a dose of UVA capable of causing erythema.

Using Equations [1] and [2] (Supporting Information), the residual percentage of SPF in vitro (% $SPF_{eff.}$) and UVAPf (% $UVAPf_{eff.}$) were obtained and are listed in Table 4: if greater than or equal to 80, they can classify a filter as being photostable, according to the regulatory aspect [42].

In terms of %SPFeff. all compounds showed complete photostability. It should be noted that for compound **BZTidr9**, **BZTidr10** and **BZTidr11** a noteworthy increment in the UVAPF after irradiation was recorded. However, this unexpected behaviour was not coupled with λ_{max} values shifting for any of those compounds (*data not shown*), which could have been related to photoisomerization processes.

2.3.4. Booster activity

In order to fully understand the photoprotective profile of the benzothiazole candidates for sunscreen activity, we subdued our candidates to a booster effect evaluation test, a very appreciated approach to achieve similar SPF values but with lower filter concentrations. During the formulation stage of a sunscreen product, those ingredients that lead to an increment of the final SPF or UVAPf value are defined as UV-boosters as they can enhance the UV protection of the product. Boosters can be small molecules, polymers, or nanosized particles, that could act on the rheological properties of the formulation, on the solubilization of the filter, or can synergistically interact with UV filters through antioxidant mechanisms, for example, quenching of ROS produced upon filter photoexcitation, or photochemical mechanism, like triplet-triplet quenching, or they can preserve the UV-filter itself from degradation [43].

We decided to subject only candidates showing the best antioxidant and photoprotective activity in the previously conducted test to booster activity evaluation; also, limited cytotoxic effects on healthy keratinocytes was considered a mandatory requirement in the view of a topical skin application of those potential UV filters. Thus, compounds **BZTidr8**, **BZTidr10** and **BZTidr12** were incorporated at 3 % concentration into a standard sunscreen formulation (SSF) with labelled SPF and UVAPF values of 30 and 10, respectively, and the photoprotective parameters were evaluated pre- and post-irradiation with a solar simulator as described above. Results are listed in Table 5.

The SSF alone shows minimal photosensitivity and loses almost 18 % of its SPF value and 11 % of UVAPf value during sunlight irradiation, thus maintaining at least 80 % of its photoprotective potential. Therefore, it can be considered photostable. Outcomes of the recorded spectra show that benzothiazole derivatives **BZTidr8**, **BZTidr10** and **BZTidr12** were able to moderately increase the SPF of the sunscreen formulation, with new SPF values ranging from 50.65 (19.94 % increase) to 56.87 (34.67 % increase), and slightly increase the UVAPf, with new values recorded in the range between 13.69 (12.86 % increase) and 14.15 (16.65 % increase). It is also worth mentioning that selected

Table 3
Photoprotective parameters for benzothiazole compounds **BZTidr7-12** at 3 % in O/W sunscreen formulation.

Compound	SPF	UVAPF	UVA/UVB	λc[a] (nm)	CoV%
BZTidr7	1.88	2.18	1.21	381	0.88
BZTidr8	4.93	6.02	1.42	372	1.66
BZTidr9	3.44	3.31	1.50	371	1.00
BZTidr10	4.53	7.61	1.69	374	1.56
BZTidr11	1.87	2.90	1.52	375	1.15
BZTidr12	3.40	5.67	1.59	374	0.91
BZTidr4	1.53	1.65	1.05	389	0.61
PBSA	*1.91*	*1.13*	*0.67*	*357*	*0.32*

[a] Wavelength at which the integral of the spectral absorbance curve reaches 90 % of the area under the curve from 290 to 400 nm. For each sample, five consistent measurements with a CoV% value < 3 % were selected. Each value is the mean of at least three independent experiments. The standard deviation is not shown in the table as it was less than 10 % in all cases.

Table 4
Photostability parameters of benzothiazole hydrazones **BZTidr7-12** calculated with equations [1] and [2]. For each sample, five consistent measurements with a CoV% value < 3 % were selected. Each value is the mean of at least three independent experiments. The standard deviation is not shown in the table as it was less than 10 % in all cases.

Compound	%SPFeff.	%UVAPfeff.
BZTidr7	102.17	106.42
BZTidr8	104.00	99.00
BZTidr9	104.56	127.79
BZTidr10	106.65	206.40
BZTidr11	105.05	167.93
BZTidr12	102.26	103.88
PBSA	103.66	100.00

Table 5
Photoprotective parameters of selected benzothiazole derivates at 3 % concentration in a standard sunscreen formulation (SSF). For each sample, five consistent measurements with a CoV% value < 3 % were selected. Each value is the mean of at least three independent experiments. The standard deviation is not shown in the table as it was less than 10 % in all cases.

Condition	*Pre-irradiation*			*Post-irradiation*				
UV-parameter	**SPF**	**UVAPf**	**CoV%**	**SPF**	**UVAPf**	**CoV%**	**%SPF$_{eff.}$**	**%UVAPf$_{eff.}$**
SSF	42.23	12.13	1.57	35.00	10.88	1.99	82.87	89.69
SSF + BZTidr8 (3 %)	50.65	13.69	1.18	41.10	11.96	1.75	81.14	87.36
SSF + BZTidr10 (3 %)	52.97	13.89	1.78	47.05	12.98	2.03	88.82	91.73
SSF + BZTidr12 (3 %)	56.87	14.15	2.77	47.00	13.13	2.27	82.64	92.79

benzothiazoles did not affect the photostability of the sunscreen formulation, which was in some cases even improved (i.e., compound **BZTidr10**).

2.4. Antiproliferative activity on Colo38 and HaCat

All synthesized compounds were assayed for antiproliferative activity in vitro. To obtain a cytotoxicity and selectivity profile, immortalized human HaCat keratinocytes were used as control while the Colo38 cutaneous melanoma cell line was chosen as the skin tumor model. The data are reported as IC_{50} μM values and are accompanied by the selectivity index (SI), shown in Table 6. Cisplatin was utilized as positive control for HaCat cells, while a previously evaluated benzimidazole hydrazone derivative [14] was used as positive control for Colo38 cells.

Non-substituted or mono-substituted derivatives did not show any antiproliferative activity up to 100 μM, which was the highest concentration tested. Benzothiazole hydrazones **BZTidr10**, **BZTidr11** and **BZTidr12** were active against Colo38, although only at high concentrations (54.61–81.30 μM). Compounds **BZTidr10** and **BZTidr11** were also able to inhibit HaCat proliferation, again at very high concentrations (89.27 and 80 μM) in comparison to known antineoplastic drugs such as cisplatin (IC_{50} = 2 μM). Even if the SI was found to be favorable (1.63 and 1.08, respectively) it is not sufficient to consider those derivatives as potential antitumoral agents, as it was suggested by Indrayanto et al. [44] that a SI equal or superior to 3 is desirable in order to classify a prospective anti-cancer sample, in analogy with the previous acyl-hydrazone series (**BZTidr4**). From these results, compounds bearing a catechol or a 3-methoxy-4-hydroxy substitution pattern on the aromatic ring were found to have the most interesting antiproliferative profile. The complete absence of antiproliferative activity of compounds **BZTidr7**, **BZTidr8**, **BZTidr9** and **BZTidr12** on HaCat cells is of greatest interest in view of a topical vehiculation of those multifunctional candidates.

Table 6
Antiproliferative activity of benzothiazole derivatives towards human melanoma Colo-38 and the keratinocyte cell line HaCat.

Compound	Colo38 (IC_{50}, μM)[a]	HaCat (IC_{50}, μM)[a]	SI
BZTidr7	> 100	> 100	-
BZTidr8	> 100	> 100	-
BZTidr9	> 100	> 100	-
BZTidr10	54.61 ± 12.21	89.27 ± 33.72*	1.63
BZTidr11	74.00 ± 12.97*	80.04 ± 12.26*	1.08
BZTidr12	81.30 ± 8.98	> 100	> 1.23
BZTidr4	92.61	> 100	1.08
Cisplatin	NT[b]	**2.00 ± 0.40**	-
[Cmp 13][c]	**0.70 ± 0.06**	NT[b]	-

Statistical differences between treated and negative control groups were assessed using a two-tailed unpaired *t*-test with Welch's correction.
BZTidr10 Colo38: $t(2.0) = 7.48$; $p = 0.0174$. HaCat: $t(2.0) = 0.55$; $p = 0.06369$
BZTidr11 Colo38: $t(4.0) = 3.47$; $p = 0.0739$. HaCat: $t(2.0) = 2.82$; $p = 0.1061$
BZTidr12 Colo38: $t(2.0) = 3.80$; $p = 0.0628$. HaCat: -
Significance levels: * $p < 0.05$.
[a] Each value is the mean of at least three independent experiments (mean ± SD).
[b] Not tested.
[c] N^1-(4-arylidene)-1H-(2-OH-4-N(Et)$_2$-phenyl)-[*d*]imidazole-2-carbohydrazide [14]

2.5. In vitro inhibition of purified tyrosinase

Compounds that showed lower IC_{50} values in Colo 38 than in HaCa cells were further investigated to evaluate their potential activity as tyrosinase inhibitors, given the well-established correlation between tyrosinase activity, melanogenesis, and melanoma [45–49]. **BZTidr10–12** were tested against isolated tyrosinase in a concentration range of 0.1–100 μM, showing a comparable percentage of relative inhibition across all three inhibitors tested (Table 7).

Notably, tyrosinase inhibition activity reached a plateau at concentrations ≥ 20 μM (Table 7), a finding that may suggest a positive correlation between the inhibitory effect on tyrosinase and the observed anti-melanoma activity in Colo 38 cells, and which requires further investigations. Nevertheless, the inhibitory activity of **BZTidr10–12** against tyrosinase suggests an additional expansion of their multifunctional profile, potentially as skin lightening agents.

2.6. Anti-inflammatory activity

Next, the compounds were tested for their anti-inflammatory potential *in vitro*. As inflammation is considered a driving factor for many diseases like atherosclerosis, cancer, and infective diseases and since it can be triggered by UV radiation overexposure, we evaluated the benzothiazole derivatives as potential inhibitors of antioxidant-sensitive pro-inflammatory enzymes that are able to form lipid mediators (LM) involved in skin-inflammatory processes.

2.6.1. Screening for modulation of LM formation in monocytes

To gain insights into the anti-inflammatory properties of benzothiazole derivatives **BZTidr7–12**, we conducted a screening using

Table 7
Inhibition profile of **BZTidr10-12** against isolated tyrosinase. Each value is the mean of at least three independent experiments (mean ± SD). Kojic acid (data not shown) was used as a reference inhibitor and tested at 0.75 mM, under the same experimental conditions, to identify the range of temporal linearity (over 40 min) on the inhibition trend.

Compound	Concentration (μM)	% RI
BZTidr10	1	3.46 ± 0.13
	10	5.52 ± 0.73
	20	95.34 ± 0.00
	50	93.78 ± 2.54
BZTidr11	1	2.94 ± 0.26
	10	1.19 ± 0.00
	20	96.89 ± 9.52
	50	102.07 ± 0.73
BZTidr12	1	3.59 E(−14) ± 0.00
	10	1.04 ± 0.07
	20	101.81 ± 1.83
	50	102.07 ± 0.92

primary human monocytes. These innate immune cells express the key LM-biosynthetic enzymes required to produce pro-inflammatory PGE_2, 12-HETE, 5-HETE, and LTB_4 (Fig. 1A). To induce formation of these LM after preincubation with the test compounds at 10 μM or with the reference COX inhibitor diclofenac (1 μM), cells were treated with 2.5 μM Ca^{2+}-ionophore (A23187) for 30 min. AA substrate liberation was only affected by the reference inhibitor diclofenac ($p = 0.03$) – most likely because of diminished utilization by COX – but not by the compounds **BZTidr7–12** (Fig. 1B). Similarly, the production of PGE_2 was inhibited only by diclofenac (80 % inhibition; $p < 0.0001$). In contrast, **BZTidr10** and **BZTidr12** significantly increased formation of PGE_2 by 62 % ($p = 0.008$) and 53 % ($p = 0.017$), respectively (Fig. 1C).

Interestingly, all test compounds significantly and robustly inhibited the production of 5-LO products, including LTB_4 (inhibition > 90 %; p values ranging between 0.022 and less than 0.0001) (Fig. 1D) and 5-HETE (inhibition > 75 %; $p < 0.0001$) (Fig. 1E). In contrast, the activity of other lipoxygenases was less affected by the test compounds. As shown for 12-LO, only **BZTidr9**, **10**, and **12** weakly (inhibition < 38 %; $0.003 < p < 0.013$) reduced 12-HETE formation (Fig. 1F).

2.6.2. 5-LO inhibition in cell-free and cell-based assays

5-LO plays an essential role in the biosynthesis of leukotrienes (LTs), pro-inflammatory mediators involved in the inflammatory process of a number of severe conditions like atherosclerosis, asthma, and cancer [50]. As a dioxygenase, 5-LO performs two distinct enzymatic activities resulting in the formation of LTA_4 that is further converted to LTB_4 and/or cysteinyl-LTs depending on the cell type [51].

Prompted by the robust inhibition observed in primary human monocytes, the ability of compounds **BZTidr7–12** to inhibit 5-LO was further explored using A23187-stimulated human polymorphonuclear leukocytes (PMNL), a widely used cell model for assessing 5-LO inhibitors [52]. Additionally, a cell-free assay was employed in order to determine the direct impact of **BZTidr7–12** on 5-LO enzyme activity (Fig. 2).

Inhibition of 5-LO product formation could be confirmed for all benzothiazole hydrazones (**BZTidr7–12**) in both the cell-free (isolated 5 LO) and cell-based (PMNL) assay. At 10 μM, all hydrazone-linked compounds completely inhibited formation of 5-LO products. The degree of inhibition was similar or superior to the FDA approved 5-LO inhibitor zileuton at the same concentration (Table 8). In cell-based assays, the IC_{50} values ranged from 0.33 to 3.12 μM, with **BZTidr12** being the most potent 5-LO inhibitor ($IC_{50} = 0.33$ μM; 95 % confidence interval = 0.24–0.42 μM). Similarly, **BZTidr12** proved to be the strongest inhibitor of isolated 5-LO activity in the cell-free assay, with an IC_{50} of 0.03 μM (95 % confidence interval = 0.02–0.03 μM) (Table 9). Like the effect of compounds **BZTidr7–12** regarding their antioxidant behavior, the choice of the linker structure proved to be paramount for 5 LO inhibition, rather than the choice of the substitution pattern of the aromatic ring. These results reveal **BZTidr7–12** to be strong, direct inhibitors of 5-LO activity, likely governed through interference with the redox state of the enzyme.

2.6.3. ROS production in neutrophils

5-LO activity depends on many different processes, including the local redox-state [51]. Since compounds **BZTidr7–12** inhibit 5-LO activity and also display antioxidant activity, we next investigated their ability to modulate intracellular ROS. ROS production in PMNL was induced by phorbol-12-myristate-13-acetate (PMA), a well-known agonist for inducing ROS formation [53]. Dichlorofluorescein diacetate (DCF-DA) was used as cell-permeable and ROS-sensitive dye to assess intracellular ROS levels; diphenyliodonium chloride (DPI, 10 μM) was used as positive control. This assay allows the evaluation of possible interaction of **BZTidr7–12** with intracellular ROS production and the compounds' ability to function as radical scavengers in the cellular context. Accordingly, this assay provides further mechanistic information regarding the possibility of 5-LO inhibition via redox-interference.

Interestingly, although compounds **BZTidr7–12** perform very similar in terms of LM modulation, their influence on ROS production differs substantially (Fig. 3A). At 10 μM, neither **BZTidr7** nor **BZTidr9** exhibited any influence on PMA-induced ROS production in PMNL. In

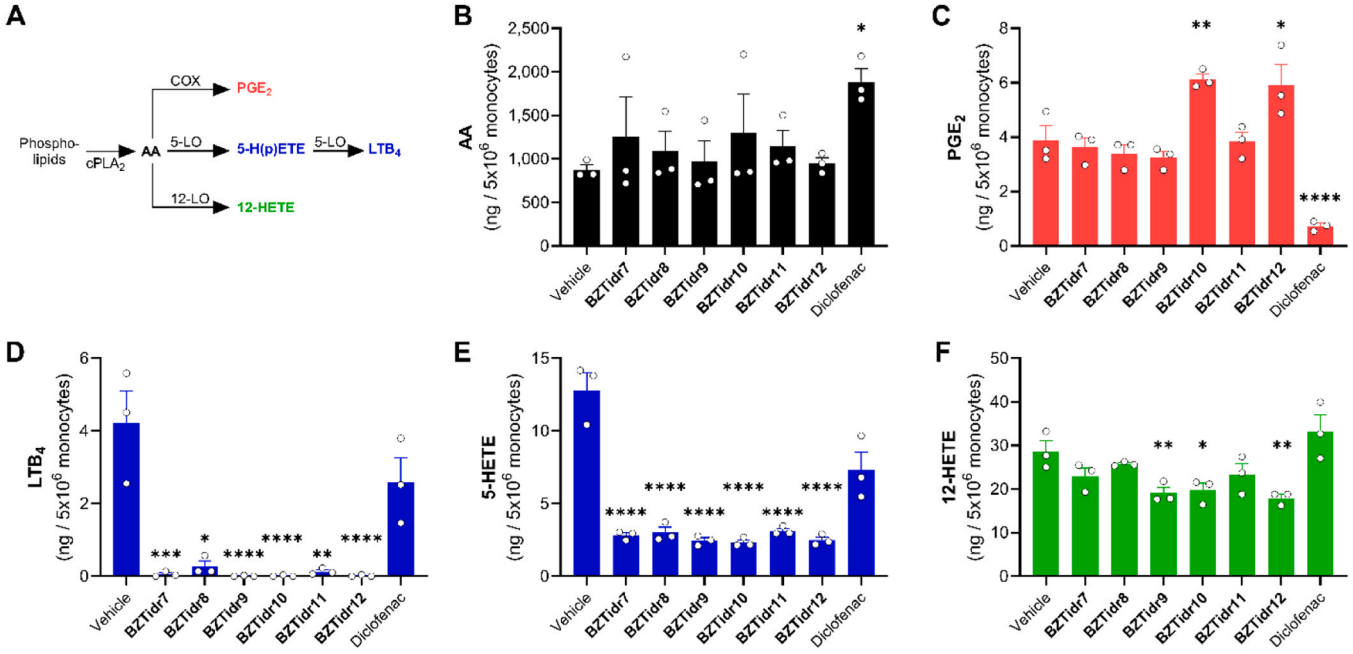

Fig. 1. Modulation of the LM profile of activated primary human monocytes by compounds **BZTidr7–12**. Primary human monocytes were pre-treated with compounds **BZTidr7–12** (10 μM), diclofenac (1 μM) or vehicle control (DMSO), followed by stimulation with A23187 (2.5 μM) for 30 min. (A) Schematic of LM biosynthetic pathways. Resulting levels of (B) substrate AA ($F_{treatment} = 2.1$; $F_{inter\text{-}donor} = 5.8$), (C) PGE_2 ($F_{treatment} = 62$; $F_{inter\text{-}donor} = 5.4$), (D) LTB_4 ($F_{treatment} = 18.8$; $F_{inter\text{-}donor} = 2.6$), (E), 5-HETE ($F_{treatment} = 38.3$; $F_{inter\text{-}donor} = 0.7$), and (F) 12-HETE ($F_{treatment} = 8.6$; $F_{inter\text{-}donor} = 3.4$) measured using UPLC-MS/MS. Data are given as means ± SEM of three independent experiments (N = 3). * $p < 0.05$; ** $p < 0.01$ *** $p < 0.001$; **** $p \leq 0.0001$ (as determined by one-way ANOVA on log-transformed data [$F_{treatment}$ (7, 14); $F_{inter\text{-}donor}$ (2, 14)], followed by Dunnett's multiple comparison test, versus vehicle with a single pooled variance).

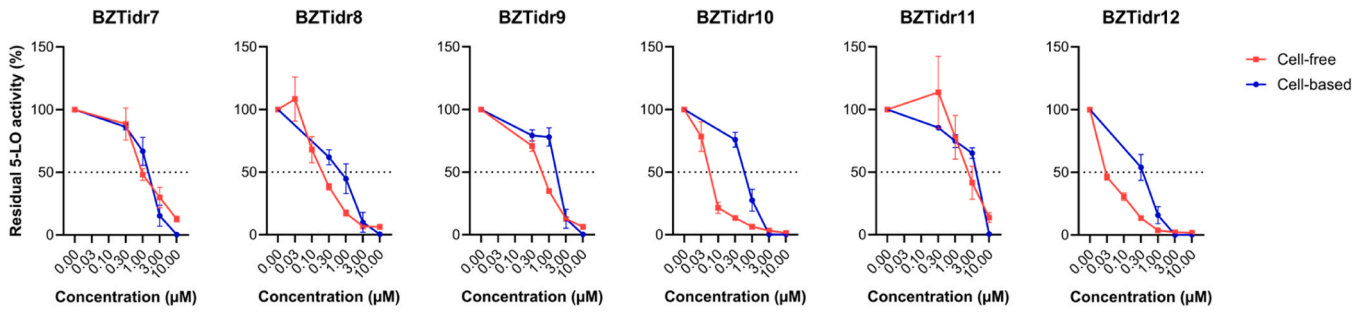

Fig. 2. 5-LO inhibition by compounds **BZTidr7–12** in a cell-based (PMNL; blue) and cell-free (isolated 5-LO; red) environment. PMNL (5 ×106/mL) or isolated 5-LO were incubated with compounds **BZTidr7–12** for 10 min before stimulating 5-LO product formation using 2.5 μM A23187 (PMNL) or 2 mM $CaCl_2$ and 20 μM AA (isolated 5-LO) for 10 min. Formed 5-LO products were measured using UPLC-MS/MS. Data are given as means ± SEM of three independent experiments (N = 3).

Table 8
5-LO inhibition values, expressed as residual enzymatic activity (%) relative to vehicle (= 100 %) at 10 μM of test compound in activated PMNL, and respective IC_{50} values.

Cmp	5-LO residual activity (PMNL, 10 μM)[a]	5-LO PMNL IC_{50} (μM)[b]	95 % CI (μM)[c]
BZTidr7	1.46 ± 0.08	1.33	[1.02 – 1.71]
BZTidr8	0.97 ± 0.43	0.58	[0.34 – 0.88]
BZTidr9	0.49 ± 0.12	1.53	[1.17 – 1.98]
BZTidr10	0.49 ± 0.17	0.57	[0.47 – 0.69]
BZTidr11	2.18 ± 0.45	3.12	[2.08 – 4.44]
BZTidr12	1.22 ± 0.42	0.33	[0.24 – 0.42]
BZTidr4	73.8 ± 26.33	-	-
Zileuton[d]	31.26 ± 12.69	-	-

[a] % relative to vehicle (DMSO). [b] IC_{50} values (μM) are the mean of three independent experiments (N = 3; DF = 13). [c] CI: confidence interval for IC_{50} values. [d] 3 μM. [Inhibitor] vs. normalized response (variable slope).

Table 9
5-LO inhibition values, expressed as residual enzymatic activity (%) relative to vehicle (= 100 %) at 10 μM of the test compounds in a cell-free assay, and respective IC_{50} values for selected compounds.

Cmp	5-LO residual activity (cell-free, 10 μM)[a]	5-LO cell-free IC_{50} (μM)[b]	95 % CI (μM)[c]
BZTidr7	16.89 ± 6.09	1.22	[0.82, 1.81]
BZTidr8	6.00 ± 1.15	0.22	[0.17, 0.29]
BZTidr9	5.33 ± 3.52	0.61	[0.55, 0.69]
BZTidr10	3.11 ± 0.38	**0.06**	[0.05, 0.07]
BZTidr11	9.34 ± 4.08	2.50	[1.28, 5.44]
BZTidr12	2.44 ± 1.14	**0.03**	[0.02, 0.03]
BZTidr4	6.32 ± 0.64	0.29	[0.18, 0.51]
Zileuton[d]	28.64 ± 7.38	-	-

[a] % relative to vehicle (DMSO). [b] IC_{50} values (μM) are the mean of three independent experiments (N = 3; DF = 13) except for **BZTidr8**, **10**, and **12**, for which three additional experiments were performed at lower concentrations due to their higher potency (N = 6; DF = 28). [c] CI: confidence interval for IC_{50} values. [d] 3 μM.

contrast, compounds **BZTidr8** and **BZTidr10–12** caused inhibition of PMA-induced ROS formation at 10 μM, reducing ROS production to 64 %, 12 %, 71 %, and 42 %, respectively (Table 10). Notably, **BZTidr10**, containing a catechol moiety, exhibited a more potent inhibitory effect on ROS formation compared to the established ROS formation inhibitor DPI (16 % residual formation at 10 μM). Given the significant inhibitory effect, further investigation was conducted on the capacity of **BZTidr10** to modulate ROS production at lower concentrations (Fig. 3B). The IC_{50} of **BZTidr10** with respect to ROS production was determined to be in the low micromolar range (2.43 μM; 95 % confidence interval = 1.54–3.93 μM).

3. Conclusion

Here, we explored of novel multifunctional compounds for their potential to interfere with different biological actions, aimed at advancing the treatment and prevention of high-incidence skin conditions such as melanoma and non-melanoma skin cancers. The primary preventive measure against these diseases remains protection from UV radiation and its associated effects, including photocarcinogenesis and oxidative degeneration. To date, no globally approved sunscreen can effectively combine both broad-spectrum UV protection and robust antioxidant activity. Therefore, the objective of this project was to develop a compound with outstanding UV-filtering and antioxidant properties, capable of mitigating or counteracting UV-induced inflammation, oxidative damage, and photo-induced neoplastic processes.

To further refine the multifunctional profile of benzothiazole-based scaffolds, we investigated the impact of linker truncation on redox behavior and various biological activities. In contrast to the previously reported acyl-hydrazone derivatives (**BZTidr1–6**) [34], the current series (**BZTidr7–12**) incorporates an imine–hydrazone bridge, which shortens the π-conjugated system and alters electronic distribution along the molecule. This structural modification was designed to shift electron density toward the benzothiazole nucleus, improving both redox reactivity and target engagement [50,54,55]. The resulting analogues demonstrated a 10- to 45-fold increased potency in 5-LO inhibition—-with **BZTidr10** showing an IC_{50} of 0.06 μM compared to 2.7 μM for its acyl-linked predecessor [34]—alongside markedly enhanced ORAC, reflecting superior anti-inflammatory and antioxidant potential. Notably, these effects were achieved without alteration of the catecholic substitution on the aryl ring, allowing isolation of the linker geometry's contribution to activity. These data support a distinct redox-interference mechanism that transcends mere additive effects from known antioxidant motifs, underscoring the critical role of linker design in conferring multifunctionality. Thus, our findings advance the understanding of benzothiazole hydrazone derivatives as multifunctional drugs and provide a chemically straightforward yet functionally impactful strategy for enhancing both anti-inflammatory and photoprotective efficacy. In fact, these compounds demonstrated excellent filtering parameters, broad-spectrum suitability, and photostability, with **BZTidr8, BZTidr10,** and **BZTidr12** enhancing SPF when combined with commercial sunscreens. The hydrazone linker, particularly when paired with a hydroxyl group in position 4 and an additional hydroxyl or methoxy group in position 3, emerges as a highly promising scaffold for further research into multifunctional UV-filter candidates, given the range of beneficial properties demonstrated in this study. Moreover, the positive correlation between the inhibitory effect on tyrosinase and the observed anti-melanoma activity in Colo 38 cells suggest tyrosinase inhibition as possible underlying mechanism.

Our results indicate that some of the synthesized compounds may inhibit 5-LO activity through modulation of the intracellular redox environment, potentially preserving the catalytic ferrous iron in its

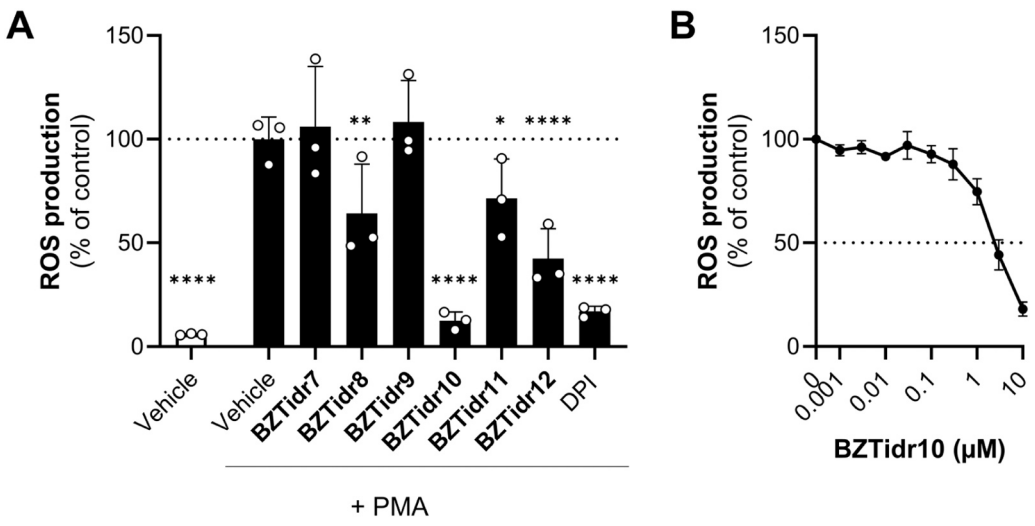

Fig. 3. ROS production (% of vehicle control) in PMNL treated with vehicle (DMSO), compounds **BZTidr7–10** (10 μM or the indicated concentrations) or DPI (10 μM, reference compound) for 10 min prior to stimulation with PMA (1 μg/mL). * $p < 0.05$; ** $p < 0.01$ *** $p < 0.001$; **** $p \leq 0.0001$ as determined by one-way ANOVA [$F_{\text{treatment}}$ (8, 16) = 41.8; $F_{\text{inter-donor}}$ (2, 16) = 12.6] followed by Dunnett's multiple comparison test vs. stimulated vehicle with a single pooled variance. (A) Screening of **BZTidr7–12** and (B) concentration-response curve for the most active compound **BZTidr10**. Results are shown as mean ± SEM of three independent experiments (N = 3).

Table 10
Impact of test compounds (10 μM) on ROS production (% of control) in PMA-stimulated PMNL (= 100 %). Mean ± SD of at least three independent experiments.

Compound	ROS production (% of control)
BZTidr7	106.05 ± 28.96
BZTidr8	64.22 ± 23.77
BZTidr9	108.37 ± 19.95
BZTidr10	**12.42 ± 4.25**[a]
BZTidr11	71.43 ± 18.95
BZTidr12	42.43 ± 14.41
BZTidr4	55.94 ± 35.54
DPI	16.44 ± 2.14

[a] IC_{50} value [95 % CI] = 2.43 [1.54–3.93] μM (N = 3; DF = 28).

reduced state. Conversely, compounds that do not markedly influence ROS levels may act via a more direct mechanism. While these observations suggest the possibility of a dual mode of action—redox interference and direct enzymatic 5-LO inhibition—we stress that this remains a *working hypothesis* based on indirect evidence. Further clarification of the binding mode will require targeted enzyme kinetic studies and computational modelling, which are planned as part of a follow-up investigation.

4. Experimental

4.1. General

All reagents were purchased from Sigma Aldrich SRL, Milano, Italy. All solvents used were purchased from Carlo Erba Reagents SRL, Milano, Italy, and used without further purification. Silica gel plates were used to perform TLC analysis (Macherey-Nagel Poligram SIL G/UV2540.20 mm, GmbH & Co. KG Neumann-Neander-str. 6–8, Dueren, Germany) and visualized by a UV lamp with the wavelength fixed to 254 nm and/or with a solution of $KMnO_4$ (1 %). Molecular weights were determined by ESI-MS (Micromass ZMD 2000) and the values are reported as $[M+H]^+$. IR spectra were registered with a Spectrum 100 FT-IR Spectrophotometer (PerkinElmer) and the main band is reported as cm^{-1}. Melting points were determined by a Stuart melting point apparatus. ^{1}H-NMR and ^{13}C-NMR were registered on the VXR-200 Varian spectrometer at 200 MHz and 400 MHz, using TMS (Tetramethylsilane) as an internal standard. The chemical shift of each signal is expressed as units δ (ppm) relative to the signal of deuterated solvents used (DMSO-d_6 and $CDCl_3$). The following abbreviations are used to designate multiplicity and assignment: s (singlet), d (doublet), t (triplet), m (multiplet), dd (double doublet), BZT (benzothiazole), and Ar (Aryl). UV spectrophotometric analysis was conducted on a UV-Vis spectrophotometer (UV-31 SCAN ONDA Spectrophotometer, Giorgio Bormac spectrophotometer Srl, Carpi (MO), Italy) or on a UV-Vis spectrophotometer (Shimadzu UV-2600). WW5 PMMA plates have been purchased from Schonberg GmbH (Munich, Germany). HPLC analysis was performed using an Agilent 1100 Series HPLC System equipped with a G1315A DAD and with a Luna® C18(2) Å column (4.6 ×150 mm, 5 μm) from Phenomenex. Chromatogram of each compound (Supporting Information) was monitored with absorbance detection at 220 ± 8 nm. The elution was performed on a gradient solvent using water (0.1 % TFA) as solvent A and acetonitrile (0.1 % TFA) as solvent B. The ratios were as follows: 95:5 (A/B) to 0:100 (A/B) in 25 min, 0:100 (A/B) to 95:5 (A/B) in 5 min, held for 2 min as post-time. The flow rate was 0.7 mL/min at room temperature. The injection volume for all samples and standards was 5 μL.

4.2. Chemistry

4.2.1. Synthesis of benzo[d]thiazole-2-thiol (2)

To a solution of 2-aminothiophenol (1.065 mL, 10 mmol) in HCl 2 M (20 mL) in a 100 mL round-bottomed flask cooled with an ice bath, potassium thiocyanate (972 mg, 10 mmol) was added in two portions. The flask was then heated to 80 °C for 24 h. Reaction was monitored by TLC. After completion, the mixture was cooled to room temperature. The separated grey solid formed upon cooling was filtered on Gooch, washed with deionized water, and dried in oven overnight. After recrystallization in EtOH, the product was recovered in 84.2 % yield. Analytical data are in agreement with those reported in literature [56].

4.2.2. Synthesis of 2-hydrazineylbenzo[d]thiazole (3)

To a solution of **2** (1.2 g, 7.18 mmol) in absolute EtOH (30 mL) in a 100 mL round-bottomed flask, 25 % w/w hydrazine hydrate (5.7 mL) was added, and reaction was heated to reflux conditions for 48 h. The reaction was monitored by TLC and evolution of H_2S was detected with a

lead acetate paper. Then the flask was allowed to cool down and the solution concentrated roughly to half the initial volume under reduced pressure. After 6–8 h at 4 °C, the solid formed was filtered on Gooch and dried in oven overnight. Recrystallization from EtOH afforded desired product shaped as white needle crystals in moderate yield (54.0 %). Analytical data are in agreement with those reported in literature [57].

4.2.3. General procedure for the synthesis of benzothiazole hydrazones BZTidr7-12

To a solution of **F** (0.61 mmol) in EtOH (5 mL) in a 50 mL round-bottomed flask, heated to 60 °C, the appropriate aromatic aldehyde (0.61 mmol) was added, and the reaction stirred for 2–5 h. Reaction was monitored by TLC. When the spot of the starting material was no longer detectable, the flask was cooled to 0 °C. The solid formed upon cooling was filtered on Gooch, dried in oven overnight, then recrystallized from hot EtOH or MeOH to afford target compounds **BZTidr7–12** in almost quantitative yields.

4.2.3.1. (E)-2-(2-benzylidenehydrazineyl)benzo[d]thiazole (BZTidr7). *pale green crystals, yield: 94.2 %. m.p. 229–232 °C; IR (cm^{-1}): 3194.44, 2892.85, 1625.33, 1573.78, 1438.98, 1272.46, 893.83.* ^{1}H-NMR (400 MHz, DMSO-d_6): δ(ppm) 12.22 (s, 1H, -NH), 8.12 (s, 1H, -N = CH-), 7.75 (d, 1H, J = 7.7 Hz, BZT), 7.71–7.65 (m, 2H, Ar), 7.47–7.34 (m, 4H, 1H BZT + 3H Ar), 7.31–7.25 (m, 1H, BZT), 7.09 (t, 1H, J = 7.4 Hz, BZT). ^{13}C NMR (101 MHz, DMSO-d_6) δ (ppm)167.55, 134.78, 131.29, 130.02, 129.31, 128.73, 126.98, 126.42, 122.08, 122.07, 121.99. ESI-MS[M+H] $^+$: calculated for $C_{14}H_{11}N_3S$, 254.07, found, 254.21. HPLC: t_R 18.88 min, purity 100.00 %.

4.2.3.2. (E)-4-((2-(benzo[d]thiazol-2-yl)hydrazineylidene)methyl)phenol (BZTidr8). grey solid, yield 92.5 %, m.p. 260–263 °C, *IR (cm^{-1}): 3543.63, 2976.19, 1609.47, 1559.91, 1438.98, 1258.59, 1092.07, 828.41.* ^{1}H-NMR (400 MHz, DMSO-d_6): δ(ppm) 12.01 (s, 1H, -NH), 9.86 (s, 1H, -OH), 8.02 (s, 1H, -N = CH), 7.72 (d, 1H, J = 7.8 Hz, BZT), 7.55–7.47 (m, 2H, Ar), 7.39 (s, 1H, BZT), 7.26 (td, 1H, J_1 = 7.7 Hz, J_2 = 7.2 Hz, J_3 = 1.3 Hz, BZT), 7.11–7.00 (m, 1H, BZT), 6.86–6.75 (m, 2H, Ar). ^{13}C NMR (101 MHz, DMSO-d_6) δ (ppm)167.285, 159.490, 128.717, 126.327, 125.824, 121.901, 121.768, 116.191. ESI-MS[M+H] $^+$: calculated for $C_{14}H_{11}N_3OS$, 270.08, found, 270.23. HPLC: t_R 14.51 min, purity 100.00 %.

4.2.3.3. (E)-2-(2-(4-methoxybenzylidene)hydrazineyl)benzo[d]thiazole (BZTidr9). white crystals, yield 91.3 %, m.p. 196–199 °C; *IR (cm^{-1}): 2964.28, 2837.30, 1609.47, 1575.77, 1508.37, 1442.95, 1248.67, 1022.68, 895.81, 820.48.* ^{1}H-NMR (400 MHz, DMSO-d_6): δ(ppm) 12.07 (s, 1H, -NH), 8.06 (s, 1H, -N = CH-), 7.73 (d, 1H, J = 7.8 Hz, BZT), 7.65–7.58 (m, 2H, Ar), 7.39 (d, 1H, J = 8.0 Hz, BZT), 7.30–7.22 (m, 1H, BZT), 7.07 (td, 1H, J_1 = 7.5 Hz, J_2 = 1.2 Hz, BZT), 7.02–6.97 (m, 2H, Ar), 3.78 (s, 3H, -OCH$_3$). ^{13}C NMR (101 MHz, DMSO-d_6) δ (ppm) 167.352, 160.924, 128.549, 127.404, 126.359, 121.931, 121.857, 114.815, 55.742. ESI-MS[M+H] $^+$: calculated for $C_{15}H_{13}N_3OS$, 284.08, found, 284.43. HPLC: t_R 17.79 min, purity 97.48 %.

4.2.3.4. (E)-4-((2-(benzo[d]thiazol-2-yl)hydrazineylidene)methyl)benzene-1,2-diol (BZTidr10). pale pink solid, yield 90.9 %, m.p. 257–261 °C (dec.); IR (*cm^{-1}): 3472.22, 3242.06, 1599.55, 1557.92, 1514.31, 1452.86, 1276.43, 1119.02, 751.10.* ^{1}H-NMR (400 MHz, DMSO-d_6): δ(ppm) 11.96 (s, 1H, -NH), 9.35 (s, 1H, -OH$_p$), 9.21 (s. 1H, -OH$_m$), 7.93 (s, 1H, -N = CH-), 7.72 (d, 1H, J = 7.8 Hz, BZT), 7.38 (d, 1H, J = 8.0 Hz, BZT), 7.25 (td, 1H, J_1 = 7.7 Hz, J_2 = 1.3 Hz, BZT), 7.16 (d, 1H, J = 2.0 Hz, Ar), 7.06 (td, 1H, J_1 = 7.7 Hz, J_2 = 1.3 Hz, BZT), 6.89 (dd, 1H, J_1 = 8.2 Hz, J_2 = 2 Hz, Ar), 6.76 (d, 1H, J = 8.1 Hz, Ar). ^{13}C NMR (101 MHz, DMSO-d_6) δ (ppm)167.190, 148.048, 146.117, 126.321, 126.227, 121.885, 121.737, 120.360, 116.046, 112.833. ESI-MS[M+H] $^+$: calculated for $C_{14}H_{11}N_3O_2S$, 286.06, found, 286.24. HPLC: t_R 13.23 min, purity 98.18 %.

4.2.3.5. (E)-5-((2-(benzo[d]thiazol-2-yl)hydrazineylidene)methyl)-2-methoxyphenol (BZTidr11). pale yellow solid, yield 87.8 %, m.p. 216–219 °C; IR *(cm^{-1}): 3531.74, 3464.28, 2833.33,2769.84, 1613.43, 1573.78, 1442.95, 1437.00, 1270.48, 1115.85.* ^{1}H-NMR (400 MHz, DMSO-d_6): δ(ppm) 12.02 (s, 1H, -NH), 9.24 (s, 1H, -OH), 7.97 (s, 1H, -N = CH-), 7.73 (d, 1H, J = 7.8 Hz, BZT), 7.39 (d, 1H, J = 7.5 Hz, BZT), 7.26 (ddd, 1H, J_1 = 8.1 Hz, J_2 = 7.3 Hz, J_3 = 1.3 Hz, BZT), 7.20 (d, 1H, J = 2.0 Hz, Ar), 7.07 (td, 1H, J_1 = 7.6 Hz, J_2 = 1.2 Hz, BZT), 7.01 (dd, 1H, J_1 = 8.4 Hz, J_2 = 2.0 Hz, Ar), 6.95 (d, 1H, J = 8.4 Hz, Ar), 3.79 (s, 3H, -OCH$_3$). ^{13}C NMR (101 MHz, DMSO-d_6) δ (ppm)167.29, 149.91, 147.27, 127.65, 126.37, 121.93, 121.85, 120.16, 112.38, 56.49, 56.04. ESI-MS [M+H] $^+$: calculated for $C_{15}H_{13}N_3O_2S$, 300.08, found, 300.31. HPLC: t_R 13.42 min, purity 98.57 %.

4.2.3.6. (E)-4-((2-(benzo[d]thiazol-2-yl) hydrazineylidene)methyl)-2-methoxyphenol (BZTidr12). pink solid, yield 95.0 %. m.p. 199–202 °C; IR *(cm^{-1}): 3539.68, 2968.25, 1625.33, 1510.35, 1444.93, 1286.34, 1264.53, 1113.87, 881.93.* ^{1}H-NMR (400 MHz, DMSO-d_6): δ(ppm) 12.04 (s, 1H, -NH), 9.46 (s, 1H, -OH), 8.00 (s, 1H, -N = CH-), 7.73 (d, 1H, J = 7.8 Hz, BZT), 7.39 (d, 1H, J = 8.0 Hz, BZT), 7.30–7.22 (m, 2H, 1H BZT + 1H Ar), 7.11–7.02 (m, 2H, 1H BZT + 1H Ar), 6.82 (d, *J* = 8.1 Hz, 1H Ar), 3.81 (s, 3H, -OCH$_3$). ^{13}C NMR (101 MHz, DMSO-d_6) δ (ppm) 167.27, 148.99, 148.41, 126.33, 126.24, 121.93, 121.78, 121.39, 116.04, 109.62, 55.93. ESI-MS[M+H] $^+$: calculated for $C_{15}H_{13}N_3O_2S$, 300.08, found, 300.31. HPLC: t_R 14.90 min, purity 100.00 %.

4.3. Antioxidant activity

4.3.1. DPPH radical scavenging assay

0.750 mL of a DMSO-MeOH solution of each tested compound was mixed with 1.5 mL of 0.004 % DPPH methanolic solution. The samples, after being placed in the dark at room temperature for 30 min, are analyzed in the spectrophotometer at a wavelength of 517 nm, corresponding to the peak of maximum absorbance relative to the DPPH radical. The obtained values were then fitted to Equation [3] (Supporting Information) and transformed into percentage inhibition (%) of the radical. The compounds were first tested at a concentration of 1 mg/mL (Trolox® was used as the standard); then, for compounds that showed radical inhibition > 90 %, their IC_{50} value (expressed in μg/mL) was determined. Ferulic acid was used as a positive control. A linear regression was performed to calculate the sample concentration that could eliminate 50 % of DPPH free radicals.

4.3.2. FRAP test

The FRAP (Ferric Reducing Antioxidant Power) test, based on a colorimetric reaction, can be used to evaluate the ability of a sample, complexed with TPTZ (2,4,6-trispiridyl-s-triazine), to reduce ferric ions to ferrous ions. FRAP solution is prepared by mixing, in a 10:1:1 ratio, 0.1 M acetate buffer (pH 3.6), 10 mmol/L of TPTZ in 40 mM HCl and a 20 mM solution of $FeCl_3$, respectively. 0.1 mL of the sample solution is then incubated at 37 °C for 10 min with 1.9 mL of the FRAP solution and then analyzed with a UV-Vis spectrophotometer at a wavelength of 593 nm, relative to the maximum absorbance peak of the Fe^{2+}-TPTZ complex. Trolox® was used as the standard and ferulic acid as positive control; results are expressed in μmolTE/g.

4.3.3. ORAC assay

The ORAC assay was performed based on Hong's procedure, modified in previous work [58], using a Fluoroskan FL® Ascent (Thermo Fisher Scientific, Inc., Waltham, MA, USA) equipped with fluorescent filters (excitation wavelength: 485 nm; emission filter: 538 nm). Fluorescein sodium salt (85 nM) was used as the target of free radical attack with 2,2′-azobis(2-amidinopropane) dihydrochloride (AAPH) as the

peroxyl radical generator in the final assay mixture (total volume of 0.2 mL). Trolox was used as a standard control, with which a calibration curve in the range of 40–240 μM is constructed. The tested compounds were solubilized in DMSO-MeOH and then diluted in PBS pH 7.4. ORAC values are calculated as the difference of the areas under the fluorescein quenching curves between the blank and the sample and expressed as μmol Trolox equivalents (TE) per gram of dried sample.

4.4. Photoprotective activity

4.4.1. In vitro evaluation of filtering parameters of compounds in solution

Absorbance of synthesized compounds was measured between 290 and 400 nm using a 1 cm quartz cell at intervals of 1 nm using a UV-Vis Spectrophotometer (SHIMADZU UV-2600 240 V). Test compounds were dissolved in DMSO and suitably diluted in MeOH to a final concentration of 10 μg/mL, and the absorbance at wavelength λ is related to the transmittance T(λ) by the Equation [4] (Supporting information). Then, filtering parameters (SPF, UVAPf, UVA/UVA and ʎc) were calculated by applying Equations [5], [6] and [7] (Supporting information) using a SPF Calculator Software (SPF Calculator Software version 2.1, Shimadzu, Milan, Italy).

4.4.2. In vitro evaluation of filtering parameters of sunscreen formulations

To a suitable oil-in-water (O/W) cosmetic formulation for solar use, the synthesized compounds were incorporated at a concentration of 3 %.

INCI: Aqua, Glycerin, Xanthan Gum, Phenoxyethanol (and) Ethylhexylglycerin, Tribehenin PEG-20 Esters, Cetearyl Alcohol, Dicaprylyl Carbonate, PPG 26 Buteth-26 (and) PEG 40 hydrogenated castor oil, C12–15 Alkyl Benzoate, Sodium hydroxide (sol. 10 %).

Three PMMA plates were used as reported in a previous protocol [18]. To facilitate the formation of a standard stabilized sunscreen film, the plate was placed in the dark for 15–30 min and then inserted into the instrument for measurement. UV transmittance was measured from 290 to 400 nm at 5 different sites on each plate. The blank was prepared using a plate coated with 32.5 mg glycerin because of its non-fluorescence and UV transparency.

To evaluate the booster effect of selected synthesized compounds, they were incorporated at 3 % concentration in an oil-in-water (O/W) sunscreen formulation with fixed SPF and UVAPf values (30 and 10, respectively).

INCI: Aqua, Sodium Phytate, Alcohol, Panthenol, Glycerin, Sclerotium Gum, Xanthan Gum, Cetearyl Alcohol, Coco-glucoside, Coco-caprylate, Dicaprylyl Carbonate, Squalene, Bis-ethylhexyloxyphenol methoxyphenyl triazine, Ethylhexyl triazone, Diethylamino hydroxybenzoyl hexyl benzoate, Tocopheryl Acetate, Benzyl alcohol, Ethylhexylglycerin.

Moreover, values of in vitro SPF, UVAPF and ʎc were calculated according to Equations [5], [6] and [7] (Supporting information).

4.4.3. Photostability

Each UV filter, incorporated in an oil-in-water (O/W) emulsion, was spread on a PMMA plate and irradiated with a solar simulator by applying different doses of UVA, equivalent to an effective erythemal radiant exposure of 100 J/m^2. Photostability was assessed by analysis of the spectral transmittance, before and after irradiation, of the sunscreen thin film, measured before and after exposure to sunlight from 290 to 400 nm. The residual percentages of in vitro SPF (% SPFeff.) and UVAPF (% UVAPFeff.) were calculated according to Equations [1] and [2], (Supporting information), respectively. A filter is considered photostable if the % SPFeff. and % UVAPFeff. are greater than or equal to 80 according to current regulations [42].

4.5. Antiproliferative activity

4.5.1. Cell growth inhibition assay

Cell growth inhibition assays were carried out using human melanoma Colo38 cells [59] and skin HaCat keratinocytes [14,15]. Human melanoma Colo38 cells were kindly provided by Dr. Patrizio Giacomini (Laboratory of Immunology, Regina Elena Institute, Rome, Italy). HaCat cells were kindly provided by Istituto Zooprofilattico Sperimentale della Lombardia e dell'Emilia-Romagna, Brescia, Italy. Cells were seeded at 40,000 cells/mL and 25,000 cells/mL, respectively. Colo38 cells were maintained in RPMI 1640, supplemented with 10 % fetal bovine serum (FBS), penicillin (100 Units/mL), and streptomycin (100 μg/mL). HaCat cells were maintained in DMEM, supplemented with 10 % FBS, penicillin (100 Units/mL), streptomycin (100 μg/mL) and glutamine (2 mM); the incubation was performed at 37 °C in a 5 % CO_2 atmosphere. Test compounds were dissolved in MeOH/DMSO (1:1) to obtain 50 mM stock solutions and diluted before cell treatment in MeOH 100 %. The test compounds were added at serial dilutions to the cell cultures (from 0.1 to 100 μM) and incubated for 24 h. Cells were then harvested, suspended in physiological solution, and counted with a Z2 Coulter Counter (Coulter Electronics, Hialeah, FL, USA). The cell numbers and the IC_{50} values were determined when untreated cells were in the log phase of cell growth. Cisplatin was used as positive control for HaCat, while N^1-(4-arylidene)-1H-(2-OH-4-N(Et)2-phenyl)-[d]imidazole-2-carbohydrazide [14] was used as positive control for Colo38 cells. The selectivity index (SI) was also calculated and is the ratio between the IC_{50} of a given compound towards the non-cancerous cell line and the IC_{50} of the same compound towards the tumour cell line.

4.6. Tyrosinase activity assay

Inhibition of tyrosinase activity was assessed using the Tyrosinase Inhibitor Screening Kit MAK257 (lot number 8K21K05750, Sigma Aldrich) according to the manufacturer's instructions. Briefly, each inhibitor sample solubilized in DMSO was appropriately diluted in tyrosinase assay buffer to reach a final concentration of 0.1, 1, 10, 20, 50, 100 μM and incubated in a 96-well flat bottom clear plate with freshly prepared solutions of tyrosinase, enzyme enhancer, and substrate. The enzyme activity control and the inhibitor control were tested by replacing test-inhibitor solutions with tyrosinase buffer (blank) and a 0.75 mM kojic acid solution, respectively. The absorbance was recorded in kinetic mode for 40 min at 492 nm (Sunrise, XFLUOR4 version V 4.51, Switzerland) and the percentage of relative inhibition for each sample was calculated according to Equation 8 as reported in Supporting Information.

4.7. Anti-inflammatory activity

4.7.1. Lipid mediator formation in primary human monocytes

Human monocytes and PMNL were freshly isolated from leukocytes concentrates provided by the Institute for Transfusion Medicine of the University Hospital Jena (Thuringia, Germany) as described previously [60]. Experimental protocols involving human blood and cells were approved by the ethical commission of University Hospital Jena. Peripheral blood mononuclear cells (PBMC) were allowed to adhere for 1 h following blood density centrifugation. Subsequently, non-adherent cells were washed off from adherent monocytes, followed by pre-incubation of adherent monocytes (5 ×106 cells/mL) with the test compounds for 10 min. LM formation was elicited with A23187 (2.5 μM) in the presence of $CaCl_2$ (1 mM). LM formation was stopped after 30 min by addition of 1 mL of ice-cold methanol containing 10 μL of deuterium-labelled internal LM standards (200 nM *d*8–5S-HETE, *d*4-LTB_4, *d*5-LXA_4, *d*5-RvD2, *d*4-PGE_2 and 10 μM *d*8-AA). LMs were extracted using Sep-Pak C18 35 cc Vac Cartridges (Waters, Milford, MA, USA) and analysed by UPLC-MS/MS as previously described [61].

4.7.2. 5-LO inhibition in cell-based assay (PMNL)

After blood density centrifugation and cell population separation (see above), PMNL were obtained from the pellet after erythrocyte lysis using hypotonic treatment. Freshly isolated PMNL (10^6 cells/mL) were diluted in PBS buffer (pH 7.4), and supplemented with glucose (1 mg/mL) and $CaCl_2$ (2.5 μM). Cells were pre-incubated with test compounds for 10 min at 37 °C, followed by stimulation with A23187 (2.5 μM) and arachidonic acid (20 μM) for another 10 min. The reaction was stopped by addition of 1 mL ice-cold methanol, containing PGB_1 as an internal standard. Major 5-LO products (5-HETE, LTB_4, 6-*trans*-LTB_4 and 12-*epi*-6-*trans*-LTB_4) were extracted using Sep-Pak C18 35 cc Vac Cartridges (Waters, Milford, MA) and analyzed by UPLC-MS/MS as previously described [62].

4.7.3. 5-LO inhibition in cell-free assay (isolated enzyme)

Human recombinant 5-LO was expressed and isolated as described before [63]. Test compounds were pre-incubated with purified 5-LO (0.5 μg) in PBS (pH 7.4) containing EDTA (1 mM) for 10 min (4 °C) and subsequently pre-warmed for 30 s (37 °C). Next, 5-LO product formation was induced by sequential addition of $CaCl_2$ (2 mM) and arachidonic acid (20 μM). After 10 min, the reaction was stopped by addition of ice-cold methanol (1 mL) containing PGB_1 as internal standard. Major 5-LO products (5-HETE, 6-*trans*-LTB_4 and 12-*epi*-6--*trans*-LTB_4) were extracted using Sep-Pak C18 35 cc Vac Cartridges (Waters, Milford, MA) and analyzed by UPLC-MS/MS as previously described [49].

4.7.4. ROS production in PMNL

Freshly isolated PMNL (10^6 cells/mL) diluted in PBS buffer (pH 7.4) and supplemented with glucose (1 mg/mL) were seeded in a black-bottomed 96-well plate (100 μL) and pre-incubated with test compounds together with the peroxide-sensitive fluorescence dye DCF-DA (1 μg/mL) and $CaCl_2$ (1 mM). After 10 min (37 °C), PMA (1 μg/mL) was added to induce ROS formation. Subsequently, fluorescence (λ_{ex} = 485 nm, λ_{em} = 530 nm) was measured over a period of 12.5 min in a thermally controlled NOVOstar microplate reader (BMG Lab technologies GmbH, Offenburg, Germany).

4.7.5. Statistical analysis and IC50 calculations

Statistical significance was calculated using GraphPad (10.4.2) by one-way ANOVA on log-transformed data, followed by Dunnett's multiple comparison test with a single pooled variance. * $p < 0.05$; ** $p < 0.01$ *** $p < 0.001$; **** $p \leq 0.0001$. For the screening of LM formation in monocytes, results of three independent experiments were compared with respect to effects of treatment [$F_{\text{treatment}}$ (7, 14)], inter-donor variability [$F_{\text{inter-donor}}$ (2, 14)], and multiple comparisons of test compounds vs. vehicle control [degrees of freedom (DF) = 14]. For the screening of ROS formation in PMNL, results of three independent experiments were compared with respect to effects of treatment [F(8, 16)], inter-donor variability [F(2, 16)], and multiple comparisons of test compounds vs. stimulated vehicle control [DF = 16]. IC_{50} values were calculated by nonlinear fit of inhibitor concentrations vs. normalized response (variable slope), with DF as indicated in the respective tables. Raw values are provided in the supplementary information.

5. Limitations and outlook

This study introduces a series of benzothiazole–hydrazone derivatives with multifunctional properties relevant to topical photoprotection, including UV absorption, antioxidant activity, and 5-LO inhibition. However, several limitations warrant acknowledgment.

First, the two different proposed mechanisms of 5-LO inhibition—-through redox modulation and/or direct enzymatic interaction—remain a working hypothesis. While supported by structure–activity relationships and redox assays, the current findings lack direct biochemical validation. Specifically, enzyme kinetic studies and molecular docking simulations (e.g., using AutoDock) were not performed due to current technical constraints, and the potential impact on the redox state of 5-LO was not assessed using redox-sensitive fluorescent probes. These investigations are part of our planned follow-up strategy.

Second, although the antioxidant capacity of the compounds was robustly characterized in cell-free systems (DPPH, ORAC), intracellular ROS scavenging (conducted in PMNL) remains to be confirmed in keratinocytes or relevant cutaneous models. Similarly, the photoprotective effects demonstrated using the PMMA plate model do not fully capture the complexity of human skin architecture or metabolism.

Third, the cytotoxicity evaluation was limited to a single human keratinocyte line (HaCaT). Broader profiling across additional dermal and immune cell types, as well as assessments of potential irritancy or sensitization, are needed. No data are yet available on dermal absorption, metabolic stability, or formulation compatibility under cosmetic-use conditions.

Future work will address these gaps through: (i) mechanistic clarification using molecular docking and kinetic inhibition assays; (ii) imaging of ROS dynamics in keratinocytes exposed to UVA; (iii) testing of the lead compound in reconstructed human epidermis; and (iv) early ADME and toxicological profiling under conditions relevant to sunscreen development.

Despite these limitations, the current results provide strong preliminary evidence for the multifunctional potential of this new compound class and support its further development as a safe-by-design approach to topical photoprotection.

CRediT authorship contribution statement

Elisa Durini: Formal analysis, Data curation. **Filippo Marchetti:** Investigation, Formal analysis, Data curation. **Sofia Fagnani:** Formal analysis, Data curation. **Riccardo Barbari:** Writing – original draft, Investigation, Formal analysis, Data curation. **Oliver Werz:** Writing – review & editing, Writing – original draft, Supervision, Data curation. **Anna Baldisserotto:** Writing – review & editing, Writing – original draft, Supervision, Funding acquisition, Data curation. **Silvia Vertuani:** Writing – review & editing, Supervision. **Ilaria Lampronti:** Writing – review & editing, Methodology, Investigation, Funding acquisition. **Leonardo Montani:** Formal analysis, Data curation. **Chiara Tupini:** Investigation, Formal analysis. **Hofstetter Robert:** Writing – review & editing, Investigation, Formal analysis, Data curation. **Vera Bruggink:** Writing – review & editing, Funding acquisition, Formal analysis, Data curation. **Stefano Manfredini:** Writing – review & editing, Supervision, Funding acquisition.

Declaration of Competing Interest

The authors declare that they have no known competing financial interests or personal relationships that could have appeared to influence the work reported in this paper.

Acknowledgement

This research was funded by the University of Ferrara (grant FAR 2021 to A.B.; grant FAR 2022 to A.B.; grant FAR 2021 to I.L.; grant FAR 2023 to I.L.), by the Italia Ministero dell'Istruzione, Università e della Ricerca (PRIN 2017, Prot. no. 2017E84AA4_002). V.B. was funded by the European Union's Horizon 2020 Research and Innovation Program under the Marie Skłodowska-Curie grant agreement No. 955335. We thank the Free State of Thuringia/Thueringer Aufbaubank and the European Union/Europaeischer Fonds fuer regionale Entwicklung (2023 FGI 0012) for financial support.

Appendix A. Supporting information

Supplementary data associated with this article can be found in the

online version at doi:10.1016/j.biopha.2025.118511.

Data availability

Data will be made available on request.

References

[1] C.T. Keith, A.A. Borisy, B.R. Stockwell, Multicomponent therapeutics for networked systems, Nat. Rev. Drug Discov. 4 (1) (2005) 71–78, https://doi.org/10.1038/nrd1609.

[2] C.M. Hohl, J. Dankoff, A. Colacone, M. Afilalo, Polypharmacy, adverse Drug-Related events, and potential adverse drug interactions in elderly patients presenting to an emergency department, Ann. Emerg. Med. 38 (6) (2001) 666–671, https://doi.org/10.1067/mem.2001.119456.

[3] A.S. Reddy, S. Zhang, Polypharmacology: drug discovery for the future, Expert Rev. Clin. Pharmacol. 6 (1) (2013), https://doi.org/10.1586/ecp.12.74.

[4] R. Morphy, C. Kay, Z. Rankovic, From magic bullets to designed multiple ligands, Drug Discov. Today 9 (15) (2004) 641–651, https://doi.org/10.1016/S1359-6446(04)03163-0.

[5] R. Morphy, Z. Rankovic, Designed multiple ligands. An emerging drug discovery paradigm, J. Med. Chem. 48 (21) (2005) 6523–6543, https://doi.org/10.1021/jm058225d.

[6] A. Cavalli, M.L. Bolognesi, A. Minarini, M. Rosini, V. Tumiatti, M. Recanatini, C. Melchiorre, Multi-Target-Directed ligands to combat neurodegenerative diseases, J. Med. Chem. 51 (3) (2008) 347–372, https://doi.org/10.1021/jm7009364.

[7] J.S. Rhee, Alex Matthews, B. Neuburg, M. Logan, B.R. Burzynski, M. Nattinger, A. B. the skin cancer index: clinical responsiveness and predictors of quality of life, Laryngoscope 117 (3) (2007) 399–405, https://doi.org/10.1097/MLG.0b013e31802e2d88.

[8] F.L. Meyskens, P. Farmer, J.P. Fruehauf, Redox regulation in human melanocytes and melanoma, Pigment Cell Res. 14 (3) (2001) 148–154, https://doi.org/10.1034/j.1600-0749.2001.140303.x.

[9] T.M. Rünger, U.P. Kappes, Mechanisms of mutation formation with Long-Wave ultraviolet light (UVA), Photodermatol. Photoimmunol. Photo 24 (1) (2008) 2–10, https://doi.org/10.1111/j.1600-0781.2008.00319.x.

[10] K. Kamiński, U. Kazimierczak, T. Kolenda, Oxidative stress in melanogenesis and melanoma development, Contemp. Oncol. 26 (1) (2022) 1–7, https://doi.org/10.5114/wo.2021.112447.

[11] J. Krutmann, The interaction of UVA and UVB wavebands with particular emphasis on signalling, Prog. Biophys. Mol. Biol. 92 (1) (2006) 105–107, https://doi.org/10.1016/j.pbiomolbio.2006.02.018.

[12] T.J. McMillan, E. Leatherman, A. Ridley, J. Shorrocks, S.E. Tobi, J.R. Whiteside, Cellular effects of long wavelength UV light (UVA) in mammalian cells, J. Pharm. Pharmacol. 60 (8) (2008) 969–976, https://doi.org/10.1211/jpp.60.8.0004.

[13] L.E. Rhodes, K. Gledhill, M. Masoodi, A.K. Haylett, M. Brownrigg, A.J. Thody, D. J. Tobin, A. Nicolaou, The sunburn response in human skin is characterized by sequential eicosanoid profiles that May mediate its early and late phases, FASEB J. Off. Publ. Fed. Am. Soc. Exp. Biol. 23 (11) (2009) 3947–3956, https://doi.org/10.1096/fj.09-136077.

[14] A. Baldisserotto, M. Demurtas, I. Lampronti, M. Tacchini, D. Moi, G. Balboni, S. Vertuani, S. Manfredini, V. Onnis, In-Vitro evaluation of antioxidant, antiproliferative and Photo-Protective activities of benzimidazolehydrazone derivatives, Pharmaceuticals 13 (4) (2020) 68, https://doi.org/10.3390/ph13040068.

[15] A. Baldisserotto, M. Demurtas, I. Lampronti, M. Tacchini, D. Moi, G. Balboni, S. Pacifico, S. Vertuani, S. Manfredini, V. Onnis, Synthesis and evaluation of antioxidant and antiproliferative activity of 2-Arylbenzimidazoles, Bioorg. Chem. 94 (2020) 103396, https://doi.org/10.1016/j.bioorg.2019.103396.

[16] V. Onnis, M. Demurtas, A. Deplano, G. Balboni, A. Baldisserotto, S. Manfredini, S. Pacifico, S. Liekens, J. Balzarini, Design, synthesis and evaluation of antiproliferative activity of new benzimidazolehydrazones, Molecules 21 (5) (2016) 579, https://doi.org/10.3390/molecules21050579.

[17] M. Demurtas, A. Baldisserotto, I. Lampronti, D. Moi, G. Balboni, S. Pacifico, S. Vertuani, S. Manfredini, V. Onnis, Indole derivatives as multifunctional drugs: synthesis and evaluation of antioxidant, photoprotective and antiproliferative activity of indole hydrazones, Bioorg. Chem. 85 (2019) 568–576, https://doi.org/10.1016/j.bioorg.2019.02.007.

[18] E.N. Djuidje, S. Sciabica, R. Buzzi, V. Dissette, J. Balzarini, S. Liekens, E. Serra, E. Andreotti, S. Manfredini, S. Vertuani, Design, synthesis and evaluation of benzothiazole derivatives as multifunctional agents, Bioorg. Chem. 101 (2020) 103960.

[19] E.N. Djuidje, R. Barbari, A. Baldisserotto, E. Durini, S. Sciabica, J. Balzarini, S. Liekens, S. Vertuani, S. Manfredini, Benzothiazole derivatives as multifunctional antioxidant agents for skin damage: Structure-Activity relationship of a scaffold bearing a Five-Membered ring system, Antioxidants 11 (2) (2022) 407, https://doi.org/10.3390/antiox11020407.

[20] R. Barbari, C. Tupini, E. Durini, E. Gallerani, F. Nicoli, I. Lampronti, A. Baldisserotto, S. Manfredini, Design, synthesis and evaluation of new multifunctional benzothiazoles as photoprotective, antioxidant and antiproliferative agents, Molecules 28 (1) (2022) 287, https://doi.org/10.3390/molecules28010287.

[21] Y. Murthi, D. Pathak, Synthesis and antimicrobial screening of substituted 2-Mercaptobenzothiazoles, J. Pharm. Res 7 (3) (2008) 153–155.

[22] B. Rajeeva, N. Srinivasulu, S.M. Shantakumar, Synthesis and antimicrobial activity of some new 2-Substituted benzothiazole derivatives, J. Chem. 6 (2009) 775–779, https://doi.org/10.1155/2009/404596.

[23] M.K. Singh, R. Tilak, G. Nath, S.K. Awasthi, A. Agarwal, Design, synthesis and antimicrobial activity of novel benzothiazole analogs, Eur. J. Med. Chem. 63 (2013) 635–644.

[24] R.S. Keri, M.R. Patil, S.A. Patil, S.A. Budagumpi, Comprehensive review in current developments of Benzothiazole-Based molecules in medicinal chemistry, Eur. J. Med. Chem. 89 (2015) 207–251, https://doi.org/10.1016/j.ejmech.2013.02.027.

[25] R. Caputo, M.L. Calabrò, N. Micale, A.D. Schimmer, M. Ali, M. Zappalà, S. Grasso, Synthesis of benzothiazole derivatives and their biological evaluation as anticancer agents, Med. Chem. Res. 21 (2012) 2644–2651, https://doi.org/10.1007/s00044-011-9789-8.

[26] J. Ma, G. Bao, L. Wang, W. Li, B. Xu, B. Du, J. Lv, X. Zhai, P. Gong, Design, Synthesis, biological evaluation and preliminary mechanism study of novel benzothiazole derivatives bearing Indole-Based moiety as potent antitumor agents, Eur. J. Med. Chem. 96 (2015) 173–186, https://doi.org/10.1016/j.ejmech.2015.04.018.

[27] M.Z. Hassan, S.A. Khan, M. Amir, Design, synthesis and evaluation of N-(substituted benzothiazol-2-Yl) amides as anticonvulsant and neuroprotective, Eur. J. Med. Chem. 58 (2012) 206–213, https://doi.org/10.1016/j.ejmech.2012.10.002.

[28] K. Vishal, S. Saurabh, H. Asif, Synthesis and in vivo Anti-Inflammatory and analgesic activities of oxadiazoles clubbed with benzothiazole nucleus, Int. Curr. Pharm. J. 4 (2015) 457–461, https://doi.org/10.3329/icpj.v4i12.25597.

[29] P.S. Yadav, D. Devprakash, G.P. Senthilkumar, Benzothiazole: different methods of synthesis and diverse biological activities, Int. J. Pharm. Sci. Drug Res. 3 (1) (2011) 01–07, https://doi.org/10.25004/IJPSDR.2011.030101.

[30] D. Brash, UV signature mutations, Photochem. Photobiol. 91 (1) (2014) 15–26, https://doi.org/10.1111/php.12377.

[31] D. Ke, C. Shuai, Y. Jiewei, W. Zhiwei, L. Hong, Y. Chengqian, Y. Xuehai, X. Ruirui, Recent advances of sustainable UV shielding materials: mechanisms and applications, ACS Appl. Mater. Interfaces 17 (21) (2025) 30402–30422, https://doi.org/10.1021/acsami.5c04539.

[32] S. Nick, D. Daniele, A. Angelo, Inorganic and organic UV filters: their role and efficacy in sunscreens and suncare products, Inorg. Chim. Acta 360 (3) (2007) 794–802, https://doi.org/10.1016/j.ica.2005.12.057.

[33] S. Ou, K. Kwok, Ferulic acid: pharmaceutical functions, preparation and applications in foods, J. Sci. Food Agric. 84 (11) (2004) 1261–1269, https://doi.org/10.1002/jsfa.1873.

[34] R. Barbari, V. Bruggink, R.K. Hofstetter, C. Tupini, S. Fagnani, E. Baldini, E. Durini, I. Lampronti, S. Vertuani, A. Baldisserotto, O. Werz, S. Manfredini, Synthesis and biological activity assessment of 2-Styrylbenzothiazoles as potential multifunctional therapeutic agents, Antioxidants 13 (10) (2024) 1196, https://doi.org/10.3390/antiox13101196.

[35] P.C. Lima, L.M. Lima, K.C. da Silva, P.H. Léda, A.L. de Miranda, C.A. Fraga, E. J. Barreiro, Synthesis and analgesic activity of novel N-Acylarylhydrazones and isosters, derived from natural safrole, Eur. J. Med. Chem. 35 (2) (2000) 187–203, https://doi.org/10.1016/s0223-5234(00)00120-3.

[36] Md.N. Alam, N.J. Bristi, Md Rafiquzzaman, Review on in vivo and in vitro methods evaluation of antioxidant activity, Saudi Pharm. J. 21 (2) (2013) 143–152, https://doi.org/10.1016/j.jsps.2012.05.002.

[37] İ. Gulcin, Antioxidants and antioxidant methods: an updated overview, Arch. Toxicol. 94 (3) (2020) 651–715, https://doi.org/10.1007/s00204-020-02689-3.

[38] B.L. Diffey, J. Robson, A new substrate to measure sunscreen protection factors throughout the ultraviolet spectrum, J. Soc. Cosmet. Chem. 40 (3) (1989) 127–133.

[39] Sunscreen drug products for over-the-counter human use, Federal Register. ⟨https://www.federalregister.gov/documents/2019/02/26/2019-03019/sunscreen-drug-products-for-over-the-counter-human-use⟩ (Accessed 14 December 2023).

[40] G. Verheugen, Commission recommendation of 22 September 2006 on the efficacy of sunscreen products and the claims made relating thereto, Off. J. Eur. Union 265 (2006) 39–43.

[41] D. Garoli, M.G. Pelizzo, B. Bernardini, P. Nicolosi, M. Alaibac, Sunscreen tests: correspondence between in vitro data and values reported by the manufacturers, J. Dermatol. Sci. 52 (3) (2008) 193–204, https://doi.org/10.1016/j.jdermsci.2008.06.010.

[42] J. Hojerová, A. Medovcíková, M. Mikula, Photoprotective efficacy and photostability of fifteen sunscreen products having the same label SPF subjected to natural sunlight, Int. J. Pharm. 408 (1–2) (2011) 27–38, https://doi.org/10.1016/j.ijpharm.2011.01.040.

[43] M. Battistin, V. Dissette, A. Bonetto, E. Durini, S. Manfredini, A. Marcomini, E. Casagrande, A. Brunetta, P. Ziosi, S. Molesini, R. Gavioli, F. Nicoli, S. Vertuani, A. Baldisserotto, A new approach to UV protection by direct surface functionalization of TiO2 with the antioxidant polyphenol dihydroxyphenyl benzimidazole carboxylic acid, Nanomaterials 10 (2) (2020) 231, https://doi.org/10.3390/nano10020231.

[44] G. Indrayanto, G.S. Putra, F. Suhud, Chapter six - validation of in-Vitro bioassay methods: application in herbal drug research, in: A.A. Al-Majed (Ed.), Profiles of Drug Substances, Excipients and Related Methodology, 46, Academic Press, 2021, pp. 273–307, https://doi.org/10.1016/bs.podrm.2020.07.005.

[45] T. Pillaiyar, M. Manickam, V. Namasivayam, Skin whitening agents: medicinal chemistry perspective of tyrosinase inhibitors, J. Enzym. Inhib. Med. Chem. 32 (1) (2017) 403–425, https://doi.org/10.1080/14756366.2016.1256882.

[46] R. Logesh, S.R. Prasad, S. Chipurupalli, N. Robinson, S.K. Mohankumar, Natural tyrosinase enzyme inhibitors: a path from melanin to melanoma and its reported pharmacological activities, Biochim. Biophys. Acta Rev. Cancer 1878 (6) (2023) 188968, https://doi.org/10.1016/j.bbcan.2023.188968.
[47] L.M. Lazinski, M. Beaumet, B. Roulier, R. Gay, G. Royal, M. Maresca, R. Haudecoeur, Design and synthesis of 4-amino-2′,4′-dihydroxyindanone derivatives as potent inhibitors of tyrosinase and melanin biosynthesis in human melanoma cells, Eur. J. Med. Chem. 266 (2024) 116165, https://doi.org/10.1016/j.ejmech.2024.116165.
[48] B. Roulier, I. Rush, L.M. Lazinski, B. Pérès, H. Olleik, G. Royal, A. Fishman, M. Maresca, R. Haudecoeur, Resorcinol-based hemiindigoid derivatives as human tyrosinase inhibitors and melanogenesis suppressors in human melanoma cells, Eur. J. Med. Chem. 246 (2023) 114972, https://doi.org/10.1016/j.ejmech.2022.114972.
[49] M.A. Soares, M.A. Almeida, C. Marins-Goulart, O.A. Chaves, A. Echevarria, M.C. C. de Oliveira, Thiosemicarbazones as inhibitors of tyrosinase enzyme, Bioorg. Med. Chem. Lett. 27 (15) (2017) 3546–3550, https://doi.org/10.1016/j.bmcl.2017.05.057.
[50] O. Werz, D. Steinhilber, Therapeutic options for 5-lipoxygenase inhibitors, Pharmacol. Ther. 112 (3) (2006) 701–718, https://doi.org/10.1016/j.pharmthera.2006.05.009.
[51] O. Rådmark, O. Werz, D. Steinhilber, B. Samuelsson, 5-Lipoxygenase, a key enzyme for leukotrienebiosynthesis in health and disease, Biochim. Biophys. Acta 1851 (4) (2015) 331–339, https://doi.org/10.1016/j.bbalip.2014.08.012. Epub 2014 Aug 22.
[52] O. Werz, D. Steinhilber, Development of 5-lipoxygenase inhibitors–lessons from cellular enzyme regulation, Biochem. Pharmacol. 70 (3) (2005) 327–333, https://doi.org/10.1016/j.bcp.2005.04.018.
[53] R. Huang, L. Zhao, H. Chen, R.-H. Yin, C.-Y. Li, Y.-Q. Zhan, J.-H. Zhang, C. Ge, M. Yu, X.-M. Yang, MegakaryocyticDifferentiation of K562 cells induced by PMA reduced the activity of respiratory chain complex IV, PLoS ONE 9 (2014) e96246.
[54] R. Keri, M. Patil, S. Patil, S. Budagumpi, A comprehensive review in current developments of benzothiazole-based molecules in medicinal chemistry, Eur. J. Med. Chem. 89 (2014) 207–251, https://doi.org/10.1016/j.ejmech.2014.10.059.
[55] L. Shanshan, Shangde Liu, Duo Yuan, Renjie Liu, Lifang, X.Z. Hu, Discovery of quinazoline-benzothiazole derivatives as novel potent protease-activated receptor 4 antagonists with improved pharmacokinetics and low bleeding liability, Eur. J. Med. Chem. 280 (2024) 116980, https://doi.org/10.1016/j.ejmech.2024.116980.
[56] D. Cressier, C. Prouillac, P. Hernandez, C. Amourette, M. Diserbo, C. Lion, G. Rima, Synthesis, antioxidant properties and radioprotective effects of new benzothiazoles and thiadiazoles, Bioorg. Med. Chem. 17 (14) (2009) 5275–5284, https://doi.org/10.1016/j.bmc.2009.05.039.
[57] K.V. Sashidhara, S.R. Avula, P.K. Doharey, L.R. Singh, V.M. Balaramnavar, J. Gupta, S. Misra-Bhattacharya, S. Rathaur, A.K. Saxena, J.K. Saxena, Designing, synthesis of selective and High-Affinity Chalcone-Benzothiazole hybrids as brugia malayi thymidylate kinase inhibitors: in vitro validation and docking studies, Eur. J. Med. Chem. 103 (2015) 418–428, https://doi.org/10.1016/j.ejmech.2015.09.004.
[58] F. Pessina, K. Marazova, P. Ninfali, L. Avanzi, S. Manfredini, G. Sgaragli, In vitro neuroprotection by novel antioxidants in Guinea-pig urinary bladder subjected to anoxia-glucopenia/reperfusion damage, Naunyn. Schmiede Arch. Pharm. 370 (6) (2004) 521–528, https://doi.org/10.1007/s00210-004-0998-2.
[59] A. Baldisserotto, P. Buso, M. Radice, V. Dissette, I. Lampronti, R. Gambari, S. Manfredini, S. Vertuani, Moringa oleifera leaf extracts as multifunctional ingredients for “Natural and Organic” sunscreens and photoprotective preparations, Molecules 23 (3) (2018) 664, https://doi.org/10.3390/molecules23030664.
[60] K. Günther, C. Ehrhardt, O. Werz, P.M. Jordan, Protocol for lipid mediator profiling and phenotyping of human M1- and M2-monocyte-derived macrophages during host-pathogen interactions, STAR Protoc. 5 (3) (2024) 103142, https://doi.org/10.1016/j.xpro.2024.103142.
[61] M. Werner, P.M. Jordan, E. Romp, A. Czapka, Z. Rao, C. Kretzer, A. Koeberle, U. Garscha, S. Pace, H.E. Claesson, C.N. Serhan, O. Werz, J. Gerstmeier, Targeting biosynthetic networks of the proinflammatory and proresolving lipid metabolome, FASEB J. 33 (5) (2019) 6140–6153, https://doi.org/10.1096/fj.201802509R.
[62] H. Pein, A. Ville, S. Pace, V. Temml, U. Garscha, M. Raasch, K. Alsabil, G. Viault, C.-P. Dinh, D. Guilet, F. Troisi, K. Neukirch, S. König, R. Bilancia, B. Waltenberger, H. Stuppner, M. Wallert, S. Lorkowski, C. Weinigel, S. Rummler, M. Birringer, F. Roviezzo, L. Sautebin, J.-J. Helesbeux, D. Séraphin, A.S. Mosig, D. Schuster, A. Rossi, P. Richomme, O. Werz, A. Koeberle, Endogenous metabolites of vitamin e limit inflammation by targeting 5-Lipoxygenase, Nat. Commun. 9 (1) (2018) 3834, https://doi.org/10.1038/s41467-018-06158-5.
[63] L. Fischer, D. Szellas, O. Rådmark, D. Steinhilber, O. Werz, Phosphorylation- and stimulus-dependent inhibition of cellular 5-lipoxygenase activity by nonredox-type inhibitors, FASEB J. 17 (8) (2003) 949–951, https://doi.org/10.1096/fj.02-0815fje.